Measurement report: Changes in light absorption and molecular composition of water-soluble humic-like substances during a winter haze bloom-decay process in Guangzhou, China

Chunlin Zou[1,3], Tao Cao[1,3], Meiju Li[1,3], Jianzhong Song[1,2,4,*], Bin Jiang[1,2], Wanglu Jia[1,2], Jun Li[1,2], Xiang Ding[1,2], Zhiqiang Yu[1,2,4], Gan Zhang[1,2], Ping'an Peng[1,2,3,4]

[1]State Key Laboratory of Organic Geochemistry and Guangdong Provincial Key Laboratory of Environmental Protection and Resources Utilization, Guangzhou Institute of Geochemistry, Chinese Academy of Sciences, Guangzhou 510640, China

[2]CAS Center for Excellence in Deep Earth Science, Guangzhou 510640, China

[3]University of Chinese Academy of Sciences, Beijing 100049, China

[4]Guangdong-Hong Kong-Macao Joint Laboratory for Environmental Pollution and Control, Guangzhou 510640, China

Correspondence to: Jianzhong Song (songjzh@gig.ac.cn)

Abstract

Water-soluble humic-like substances (HULIS) absorb light in near-UV and visible wavelengths and exert significant influence on the atmospheric environment and climate. However, knowledge on HULIS evolution during haze bloom-decay process is limited. Herein, $PM_{2.5}$ samples were obtained during a winter haze event in Guangzhou, China, and light absorption and molecular composition of HULIS were investigated by UV-vis spectrophotometry and ultrahigh-resolution mass spectrometry. Compared with HULIS in clean days, the absorption coefficients (Abs_{365}) of HULIS in haze days were significantly higher but the mass absorption efficiencies (MAE_{365}) were relatively lower, suggesting diverse and dynamic absorption properties of HULIS during haze episodes. The CHO and CHON compounds were the most abundant components in HULIS, followed by CHOS, CHONS, and CHN. Haze HULIS presented comparatively higher molecular weight, lower aromaticity index (AI_{mod}), and higher O/C_w, O/N_w, and O/S_w ratios, indicating that HULIS fractions undergo relatively higher oxidation during haze days than clean days. Moreover, CHON and CHO compounds with high AI_{mod} were the major potential chromophores in HULIS and significantly contributed to HULIS light absorption. It's worth noting that the proportions of these chromophores were decreased during haze event, mainly owing to their higher oxidation during haze episode. Besides, accumulated contribution of organic compounds emitted from vehicles and formed from reactions of bio-VOCs also diluted light-absorbing compounds in haze HULIS. These findings help to understand HULIS evolution during haze bloom-decay process in the subtropic region of China.

1. Introduction

Water-soluble humic-like substances (HULIS), belonging to a class of highly complex organic compounds with physical/chemical properties similar to humic substances in natural aquatic/soil environments, which constitute 30%−70% of water-soluble organic compounds in ambient aerosols and are responsible for > 70% of light absorption (at 365 nm) in water-soluble brown carbon (BrC) (Graber and Rudich, 2006; Laskin et al., 2015; Huang et al., 2018). They are thought to be comprised of aromatic structures containing aliphatic side chains and oxygenated functional groups such as hydroxyl, carboxyl, nitrate, and organosulfate groups (Lin et al., 2012; Song et al., 2018; Zeng et al., 2020). HULIS are ubiquitously identified in atmospheric aerosols, fog, cloud, and rain water, and have been demonstrated to play significant effects on both atmospheric environment and climate (Bianco et al., 2018; Wu et al., 2018; Zhan et al., 2022). In addition, HULIS exert adverse health effects because they can enhance the oxidative potential of organic aerosols (Ma et al., 2019; Cao et al., 2021).

In recent years, severe particulate pollution (i.e., haze events) frequently occur in some developing country such as China, which has drawn extensive public and scientific concerns (An et al., 2019; Zhang et al., 2020). According to An et al. (2019), contributions of organic aerosols, including primary organic aerosols and secondary organic aerosols (SOA), are significant for severe haze events; in particular, the contribution of SOA in China is expected to continuously increase because of stronger chemical reactions in the atmosphere. HULIS are an important component in organic aerosols, which originate from a variety of primary emissions (e.g., biomass burning (BB), coal combustion, off-road engine emission) (Fan et al., 2016; Cui et al., 2019; Tang

64 et al., 2020) and secondary chemical oxidation of biogenic and anthropogenic volatile

65 organic compounds (VOCs) (Yu et al., 2016; Tomaz et al., 2018) and soot (Fan et al.,

66 2020). During the haze episode, a number of chemical processes occur in aqueous phase

67 (Wong et al., 2017; Wu et al., 2018) and gas phase (Sumlin et al., 2017), which lead to

68 significant changes in chemical composition and light absorption properties of HULIS.

69 For instance, recent studies on oxidation of BB-derived BrC have indicated that although

70 both enhancement and bleaching of BrC occur during aging, bleaching of BrC becomes

71 dominant over a long period (Fan et al., 2020; Wong et al., 2017; Ni et al., 2021).

72 However, multiphase reaction between carbonyl and amine has demonstrated rapid

73 formation of light-absorbing organic compounds (Kampf et al., 2016). Nevertheless, it

74 should be noted that these results were mainly obtained from laboratory experiments and

75 may not reflect the complex evolution behavior of BrC in atmospheric environment.

76 High concentrations of HULIS have been determined during typical haze episodes

77 in northern, eastern, and southern China (Fan et al., 2016; Zhang et al., 2020; Wang et al.,

78 2020), and have been demonstrated to significantly influence atmospheric visibility,

79 environment, and photochemical process. Guangzhou is the biggest city in the Pearl

80 River Delta (PRD), one of the most developed regions in China, and is located in the

81 subtropical zone with a population of over 18 million people (Yu et al., 2017). Although

82 a remarkable decline in atmospheric particulate matter ($PM_{2.5}$) pollution has been

83 observed in recent years owing to strict regulatory controls, O_3 and VOCs still remain at

84 higher levels and severe haze pollution caused by fine particulate matter frequently occur

85 in winter (An et al., 2019; Li et al., 2019; Yang et al., 2022). Several studies have

86 investigated the optical, chemical, and molecular properties of HULIS in the PRD region

87 (Lin et al., 2010, 2012; Fan et al., 2016; Liu et al., 2018; Jiang et al., 2020, 2021). For

88 example, the studies on the temporal variations of water-soluble HULIS in Guangzhou

89 indicated that HULIS had higher concentrations and mass absorption efficiencies

90 (MAE_{365}) in the winter, which were attributed to the increasing contribution of BB and

91 secondary nitrate formation in the winter monsoon period (Fan et al., 2016; Jiang et al.,

92 2020, 2021). In addition, the molecular composition of HULIS (and BrC) in the PRD

93 region were also investigated and demonstrated that the levels of unsaturated and

94 aromatic structures are the important factor influencing their light absorption properties

95 (Jiang et al., 2020). However, detailed information regarding the evolution of light

96 absorption and molecular composition of HULIS during haze events is still scarce.

97   Recently, ultrahigh-resolution Fourier transform ion cyclotron resonance mass

98 spectrometry (FT-ICR MS) coupled with electrospray ionization (ESI) sources has been

99 frequently employed to investigate the molecular characteristics of HULIS in ambient

100 aerosols (Song et al., 2018, 2022; Tang et al., 2020; Zeng et al., 2021). Owing to its

101 extremely high mass resolution and accuracy, this technique allows further exploration of

102 the evolution of HULIS during haze event. The present study performed comprehensive

103 characterization of HULIS in $PM_{2.5}$ collected during a haze event in Guangzhou, China.

104 The abundances and light absorption properties of HULIS were first measured, and

105 carbonaceous fractions, water-soluble ions, and levoglucosan (Lev) were determined.

106 Subsequently, four HULIS samples collected during different haze stages were analyzed

107 using FT-ICR MS operated in both ESI− and ESI+ modes. To the best of our knowledge,

108 the present study is the first to apply a combination of optical properties and molecular

109 characterization by FT-ICR MS to investigate HULIS in a haze event in the subtropical

110 zone of China. The results obtained provide novel insights into the evolution of HULIS

111 during haze event, and are important for predicting the environmental and climatic effects

112 of HULIS in South China.

2. Material and Methods

2.1. Aerosol sampling

115   The $PM_{2.5}$ samples were collected on the campus of Guangzhou Institute of

116 Geochemistry, Chinese Academy of Sciences, Guangzhou, China (23.14N, 113.35E),

117 which is an academic and residential region. Traffic emissions and residential activities

118 are the potential pollution sources in the sampling area. The 24-h $PM_{2.5}$ sampling was

119 conducted using a high-volume sampler (Tianhong Intelligent Instrument Plant, Wuhan,

120 China, with a flow rate of 1.0 $m^3 min^{-1}$) during 7 to 30 January of 2018, and a total of 24

121 samples were collected on the prebaked quartz filters (20.3 $\times$ 25.4 cm^2, Whatman,

122 Maidstone, UK). Field blank samples were collected by keeping a blank filter in the

123 sampler without pumping air. Before sampling, the filters were wrapped in aluminum foil

124 and prebaked at 450°C for 6 h to remove carbonaceous impurities. Before and after

125 sampling, the filters were weighed at 25°C and 50% RH on a microbalance (Sartorius

126 Model BP210D). The $PM_{2.5}$ concentrations were determined by weighing the filters

127 before and after collection. Finally, all filter samples were stored in a refrigerator at −20 °C

128 until analysis. The mass accuracy achieved was < 2% based on triplicate analyses of filter

129 samples. Meteorological data (http://www.wunderground.com/history/airport/ZGGG),

130 including wind speed, temperature, relative humidity, and concentrations of SO_2, O_3, and

131 NO_2, for the sampling days are presented in Figure 1 and Table S1.

2.2. Isolation of HULIS

HULIS were isolated using a water extraction and solid-phase extraction (SPE) procedure as described previously (Zou et al., 2020). This method has been used in most previous studies because of its easy operation and high reliability and reproducibility and low limit of detection (Fan et al., 2002), therefore, it was also used in this study. Briefly, portions of the PM$_{2.5}$ samples (100 cm^2) were ultrasonically extracted with 50 mL of ultrapure water for 30 min. The extracts were filtered through a 0.22-µm PTFE syringe filter to remove the suspended insoluble particles. About 50 mL of water extracts were obtained from each sample, of which 20 mL was used for the isolation and analysis of HULIS, 20 mL for analysis of water-soluble organic carbon (WSOC), and the remainded extracts for the analysis of inorganic ions, respectively. Then, the 20 mL water extracts were adjusted to pH of 2 with HCl, and loaded on a preconditioned SPE cartridge (Oasis HLB, 200 mg/6 mL, Waters, USA). The hydrophilic fraction (i.e., inorganic ions, high-polar organic acids, etc) was removed with ultrapure water, whereas the relatively hydrophobic HULIS fraction was retained and eluted with 2% (v/v) ammonia/methanol. Finally, HULIS solution was evaporated to dryness with a gentle N$_2$ stream and redissolved with ultrapure water for the analysis.

It is noted that the HULIS here is the hydrophobic portion of water-soluble organic matter, which can be isolated with different types of SPE columns (e.g., HLB, C-18, DEAE, XAD-8, and PPL) (Fan et al., 2012, 2013; Lin et al., 2012; Zou et al., 2020; Jiang et al., 2020). Although each resin type has its special chemical properties, the hydrophobic HULIS isolated with different sorbents were similar in chemical, molecular properties based on previous studies (Fan et al., 2012, 2013; Zou et al., 2020). Therefore,

for better comparison with other studies, the hydrophobic fractions isolated by SPE

methods were all termed as HULIS in the present paper.

2.3. Light absorption analysis

The absorption spectra of the WSOC and HULIS fractions were measured by a UV-

vis spectrophotometer (UV-2600, Shimadzu) between 200 to 700 nm. Each spectrum was

corrected for the filter blanks. The light absorption coefficients, absorption Ångström

exponent (AAE) and mass absorption efficiency (MAE_λ) were calculated and the detailed

methods are presented in the Supporting Information (SI).

2.4. Chemical analysis

For FT-ICR MS analysis, the HULIS samples were isolated from $PM_{2.5}$ collected

during four periods: before haze days (clean-I days, 7−12 January), haze bloom days

(haze-I days, 13−18 January), haze decay days (haze-II days, 19−24 January), and after

haze days (clean-II days, 25−30 January). A filter punch (18 cm in diameter) was taken

from every sample, and all the six samples in each period was combined for the isolation

of HULIS fractions. The obtained HULIS samples were measured with an ESI FT-ICR

MS (Bruker Daltonik GmbH, Bremen, Germany) equipped with a 9.4 T refrigerated

actively shielded superconducting magnet. The system was operated in both ESI− and

ESI+ modes. The scan range was set to m/z from 100 to 1000, with a typical mass-

resolving power >450,000 at m/z 319 with <0.2 ppm absolute mass error. The mass

spectra were calibrated externally with arginine clusters and internally recalibrated with

typical O_5-class species peaks in DataAnalysis 4.4 (Bruker Daltonics). Due to the

inherent differences in the ionization mechanisms between ESI- and ESI+ modes, the

data detected by the two ionization modes can provide complementary information on the

molecular composition of atmospheric HULIS (Lin et al., 2012; Lin et al., 2018). The

details of data analysis are provided in the SI.

The amounts of organic carbon (OC) and elemental carbon (EC) were determined by

a OC/EC analyzer (Sunset Laboratory Inc., USA) (Mo et al., 2018). The concentrations

of WSOC and HULIS were determined by a TOC analyzer (Shimadzu TOC_VCPH,

Kyoto, Japan). The water-soluble inorganic species (NO_3^-, SO_4^{2-}, Cl^-, NH_4^+, K^+, Na^+,

Ca^{2+}, Mg^{2+},) were measured with a Dionex ICS-900 ion chromatography system (Thermo

Fisher Scientific, USA) as described previously (Huang et al., 2018). The concentrations

of Lev were analyzed with a gas chromatography–MS after derivatization with BSTFA

and pyridine at 70 °C for 3 h (Huang et al., 2018). Detailed information regarding these

measurements is provided in the SI.

3. Results and Discussion

3.1. Abundance and chemical composition of PM$_{2.5}$

Figure 1 shows the meteorological conditions, PM$_{2.5}$ concentration, and

concentrations of major chemical constituents, including carbon fractions and water-

soluble inorganic ions in PM$_{2.5}$ samples obtained during a haze bloom-decay process.

Based on the variation in PM$_{2.5}$ concentration, these samples were categorized into four

groups: clean-I days (before haze, 14–24 µg m^{-3}), haze-I days (haze bloom, 45–114 µg

m^{-3}), haze-II days (haze decay, 58–115 µg m^{-3}), and clean-II days (after haze, 9–35 µg

m^{-3}). As indicated in Table S1 and Figure 1, the PM$_{2.5}$ concentrations increased from 18

± 3.3 µg m^{-3} in clean-I days to 82 ± 26 and 84 ± 22 µg m^{-3} in haze-I and haze-II days,

199 respectively, and then decreased to 21 ± 10 µg m^{-3} in clean-II days. This finding

200 obviously indicated that the average PM$_{2.5}$ concentrations during the examined haze

201 episode are higher than the second-grade national ambient air quality standard in China

202 (75 µg m^{-3}, 24 h), whereas those during clean days are lower than the first-grade national

203 ambient air quality standard in China (35 µg m^{-3}, 24 h). However, the average PM$_{2.5}$

204 concentrations during the haze event are lower than those in the cities in winter haze,

205 including Shenyang (108 µg m^{-3}) (Zhang et al., 2020), and Nanjing (123 $\pm$ 28.5 µg m^{-3})

206 (Li et al., 2020), Beijing (158 µg m^{-3}) and Xi'an (345 µg m^{-3}) (Zhang et al., 2018).

207   As shown in Table S1, the average concentrations of OC and EC were 2.2–15 and

208 0.36–2.7 µgC m^{-3} in the four stages, respectively, implying that the distinct changes in

209 OC and EC were higher during haze episodes than those in clear days. During the entire

210 study period, WSOC concentration ranged from 0.5 to 12.5 µgC m^{-3} (4.3 $\pm$ 1.2 µgC m^{-3}),

211 which contributed to 53%–57% of OC in PM$_{2.5}$. The HULIS concentration noted in the

212 present study ranged from 0.15 to 6.1 µgC m^{-3} (2.2 $\pm$ 1.9 µgC m^{-3}), which was

213 comparable to those observed in the PRD region, such as Hong Kong (2.38 $\pm$ 1.62 µgC

214 m^{-3}) (Ma et al., 2019) , Guangzhou (2.4 $\pm$ 1.6 µgC m^{-3}) (Fan et al., 2016), and Heshan

215 (2.08 $\pm$ 1.16 µgC m^{-3}) (Jiang et al., 2020), but lower than those in northern cities of

216 China, such as Xi'an (12.4 $\pm$ 6.5 µgC m^{-3}) (Huang et al., 2020), Beijing (3.79 $\pm$ 3.03

217 µgC m^{-3}) (Mo et al., 2018), and Lanzhou (4.7 µgC m^{-3}) (Tan et al., 2016). As shown in

218 Figure 1, HULIS also exhibited obvious variations during the entire sampling period. The

219 average HULIS concentration was 0.46 $\pm$ 0.22 µgC m^{-3} in clean-I days, which sharply

220 increased to 4.5 $\pm$ 1.2 µgC m^{-3} in haze-I days, then decreased to 3.1 $\pm$ 1.2 µgC m^{-3} in

221 haze-II days, and rapidly declined to 0.75 $\pm$ 0.52 µgC m^{-3} in clean-II days. This result

222   was consistent with the changing trend of WSOC, OC, and EC. In addition, the

223   HULIS/WSOC ratios were about 0.50 ± 0.13 in the $PM_{2.5}$ samples, which are in broad

224   agreement with other studies showing that HULIS is the major fraction of WSOC (Fan et

225   al., 2016; Ma et al., 2019; Jiang et al., 2020).

226   As illustrated in Figure 1, obvious variations in chemical compositions were also

227   observed in these $PM_{2.5}$ samples. Secondary inorganic aerosols (SIA) (i.e., SO_4^{2-}, NO_3^-,

228   and NH_4^+), OC, and EC exhibited a similar variation during the entire study period, and

229   their contents sharply increased from 10 January in clean-I days to 13−18 January in

230   haze-I days, then slowly decreased in haze-II days, and finally reached lower levels in

231   clean-II days. It must be noted that the increasing rate of EC was similar to that of SIA in

232   haze-I days, indicating that direct emissions and atmospheric reactions may play similar

233   roles in $PM_{2.5}$ increase during this haze bloom period. As indicated in Figure 1f, the

234   highest values of NO_3^-/SO_4^{2-} were observed in haze-I days, implying the important

235   influence of traffic exhausts in the haze bloom period (Mo et al., 2018). In addition, the

236   high NO_2 and O_3 concentrations and the stable meteorological condition with high

237   temperature also led to the outburst of fine particulate pollution in this period. During

238   haze-II days, the SIA and OM contents in $PM_{2.5}$ slowly decreased, whereas the

239   concentrations of Na^+, Cl^-, and unidentified materials in $PM_{2.5}$ increased (Figure 1e,h),

240   suggesting that local contribution weakened and regional contribution via sea salt became

241   more important (Jiang et al., 2021). This phenomenon was also observed to be consistent

242   with the changes in the pollutant sources transported by air masses. As indicated in

243   Figure S1, the $PM_{2.5}$ samples in haze-II days included some contributors transported from

244 coastal area of eastern Guangdong Province and Fujian Province, and the $PM_{2.5}$ are likely

245 to be enriched with sea salt materials and mineral dusts.

3.2. Light absorption

247 The light absorption properties of WSOC and HULIS (Figure 1d, i, j and Table S2)

248 exhibited obvious temporal variations during the sampling period. The AAE values of

249 WSOC and HULIS ranged from 4.1 to 6.4 and 5.6 to 6.6, respectively. The AAE values

250 for HULIS were obviously higher than those for WSOC in the same sample (Figure 1i),

251 indicating that light absorption of HULIS is more wavelength-dependent than that of

252 WSOC. Similar results were also observed in previous studies (Park et al., 2018; Jiang et

253 al., 2020; Cao et al., 2021). These differences could be attributed to the differences in

254 chemical composition of chromophores in WSOC and HULIS. As shown in Table S2, the

255 E_{250}/E_{365} values of HULIS (5.3−5.6) all higher than that (4.4−5.1) of WSOC, suggested

256 that the light-absorbing species in HULIS may have relative lower aromaticity and/or

257 lower molecular weight than those in WSOC (Chen et al., 2016; Li and Hur, 2017).

258 Therefore, the HULIS fractions exhibit relative higher absorption at UV and short visible

259 wavelengths and relative lower absorption at long visible wavelengths, which resulting in

260 relative higher AAE values. Moreover, the AAE values of HULIS did not present

261 significant variation during the entire haze process, which could be related with the

262 evolution of HULIS chromophores in different stages (Jiang et al., 2020; Huang et al.,

263 2018; Deng et al., 2022). At first, the enhanced oxidation of aromatic species in haze

264 days could lead to the bleaching or degradation of chromophores (a detailed explanation

265 was provided in Section 3.3), thus a less wavelength dependence (Forrister et al., 2015;

266 Zhan et al., 2022). In contrast, the outburst of secondary organic aerosols and the

272   Light absorption at 365 nm (Abs_{365}) for WSOC and HULIS were 2.5 ± 2.0 and $1.8 \pm$

273 1.6 M m^{-1}, respectively (Table S2). HULIS contributed to about 72% of light absorption

274 coefficients by WSOC, implying that they enriched the major light-absorbing

275 components in WSOC. As shown in Figure 1d, the Abs_{365} values for HULIS presented

276 obvious temporal variations. The $Abs_{365,HULIS}$ value was 0.55 ± 0.06 M m^{-1} in clean-I

277 days, which first increased to 3.4 ± 1.5 M m^{-1} in haze-I days and then slowly decreased to

278 2.6 ± 0.85 M m^{-1} in haze-II days, and finally rapidly declined to 0.64 ± 0.32 M m^{-1} in

279 clean-II days. This result was similar to the variations in the mass concentration of

280 HULIS. Furthermore, the Abs_{365} values for HULIS in Guangzhou were found to be

281 higher than those observed in southeastern Tibetan Plateau (0.38–1.0 M m^{-1}) (Zhu et al.,

282 2018), but obviously lower than those in Xi'an (7.6–36 M m^{-1}) (Shen et al., 2017) and

283 Beijing, (3.7–10.1 M m^{-1}) (Du et al., 2014).

284   In general, MAE_{365} value can be used to assess the light absorption capacity of target

285 organic compounds (Li et al., 2019). As shown in Figure 1j and Table S2, the average

286 MAE_{365} value for WSOC was 1.0 ± 0.21 m^2 gC^{-1} (0.68–1.3 m^2 gC^{-1}), nearly same to

287 1.1 ± 0.27 m^2 gC^{-1} (0.77–1.8 m^2 gC^{-1}) for HULIS, during the entire sampling period.

288 Moreover, the MAE_{365} values for HULIS measured in the present study were noted to be

289 dropped in the ranges of those determined in Beijing (1.43 ± 0.33 m^2 g C^{-1}) (Mo et al.,

290   2018), Xi'an (0.91–1.85m^2 g C^{-1}) (Yuan et al., 2021), and Hong Kong (1.84 ± 0.77 m^2

291   gC^{-1}) (Ma et al., 2019). The average MAE$_{365}$ values for HULIS exhibited some temporal

292   variations. The MAE$_{365}$ values for HULIS were 0.91 ± 0.03 and 0.95 ± 0.11 m^2 gC^{-1} in

293   haze-I and haze-II days, respectively, which were lower than those (1.3 ± 0.22 and $1.3 \pm$

294   0.27 m^2 gC^{-1}, respectively) observed in clean-I and clean-II days, suggesting that HULIS

295   have a relatively weaker light absorption capability in haze days. This finding is

296   consistent with the results reported by Zhang et al. (2017), who found that the MAE$_{365}$

297   values in the heating or non-heating seasons during hazy days were lower than those in

298   clean days. These differences in MAE$_{365}$ values may potentially contribute to the

299   enhanced oxidation reaction that was derived by the increased O$_3$ levels and high

300   temperature and relative humidity (RH) during haze days (Figure 1). This oxidation

301   process would lead the chromophores containing C=C unsaturated bond to be severely

302   degraded (Wang et al., 2017a; Zhang et al., 2017). Besides, an increase in additional

303   sources for HULIS in the study area, such as weaker or non-light-absorbing compounds

304   formed by atmospheric oxidation, could also result in weaker light absorption of HULIS

305   during the haze episode (Liu et al., 2018).

306   **3.3. Molecular evolution of HULIS during the haze process**

307   For an in-depth understanding of the variation in HULIS at molecular level during

308   the haze process, the four HULIS samples collected in different stages of the haze

309   process were analyzed by ESI FT-ICR MS in both negative and positive modes. As

310   shown in Figure 2, thousands of peaks were detected in the mass range between m/z 100

311   and m/z 700, with the high intensity ions noted within m/z 150–400. It is obvious that

312   some organic compounds with stronger arbitrary abundance were labeled, and their

313   formulas, double bond equivalent (DBE), modified aromaticity index (AI$_{mod}$), and

314   potential sources were listed in Table S3. Compounds a ($C_7H_7NO_3$) and b ($C_8H_6O_4$), both

315   have high DBE values, which might be assigned to aromatics such as methylnitrophenol

316   and phthalic acid, whereas compound d ($C_8H_{18}O_4S$) with low DBE value and high O/S

317   ratio was probably aliphatic organosulfate. According to previous studies, these organic

318   molecules might be derived from BB and diesel fuel and thereby these results suggested

319   that both BB and vehicular emissions are important sources of BrC in ambient aerosols

320   (Mohr et al., 2013; Riva et al., 2015; Blair et al., 2017). Furthermore, compound e

321   ($C_{10}H_{17}NO_7S$) and compound f ($C_{10}H_{18}N_2O_{11}S$) in Table S3 were found to be identical to

322   the oxidation products of monoterpenes, suggest that biogenic sources could contribute to

323   the formation of HULIS (Surratt et al., 2008; Wang et al., 2019). Thus, HULIS could be

324   affected by multiple sources during the haze process, possibly including BB, biogenic

325   sources, and anthropogenic emissions.

326   The identified formulas could be divided into seven compound categories, namely,

327   CHO−, CHON−, CHOS−, and CHONS− detected in ESI− mode and CHO+, CHN+, and

328   CHON+ detected in ESI+ mode. As illustrated in Figure 2, the CHO compounds were the

329   most abundant group in all the HULIS, accounting for 43%−50% and 51%−57% of the

330   overall compounds detected in the ESI− and ESI+ modes, respectively. It must be noted

331   that relatively lower contents of CHO− were detected during the haze episode (haze-I and

332   haze-II days) and CHO+ molecules in haze-I HULIS. The CHON compounds were the

333   second most abundant group in all the HULIS. As shown in Figure 2, the relative content

334   of CHON− was 23% in clean-I days, which slightly increased to 24%−25% in haze

335   episode, and then decreased to 23% in clean-II days. In contrast, the relative content of

336 CHON+ compounds was 41% in clean-I days, which increased to 45% in haze-I days,

337 then fell to 42% in haze-II days and 41% in clean-II days. Both CHOS− and CHONS−

338 compounds were identified in all the four HULIS, accounting for 19%–22% and 8%–11%

339 of the total identified compounds, respectively. The CHN+ compounds were the least

340 abundant (1.3%–3.6%) in the four HULIS samples, and were relatively higher during the

341 haze episode, especially in haze-I days.

342   Tables S4 and S5 show the relative abundance weighted elemental ratios, molecular

343 weight (MW), DBE, AI_{mod}, and carbon oxidation state (OS_C) for the identified

344 compounds in HULIS. The MW_w values for HULIS determined in the ESI− mode in

345 haze-I and haze-II days were 302 and 283, respectively, which were higher than those in

346 clean-I and clean-II days (266 and 264, respectively). Similar variation was also observed

347 for MW_w for HULIS detected in ESI+ mode (Table S5). These results clearly indicated

348 that more higher MW compounds constituted HULIS obtained during the haze episode.

349 Furthermore, the molecular properties of HULIS in different stages of haze process also

350 exhibited some observable differences. As shown in Table S4, the HULIS samples in

351 haze episode detected by ESI− mode presented relatively lower $AI_{mod,w}$ values and

352 relatively higher O/C_w, O/N_w, and O/S_w ratios than those in clean days, indicating that

353 haze HULIS exhibited relatively lower aromaticity and higher oxidation degree than

354 clean HULIS. These differences can be attributed to the enhanced oxidation degradation

355 of aromatic compounds (e.g., phenols, nitroaromatic compounds and polycyclic aromatic

356 hydrocarbons (PAHs)) during the haze process. In addition, increased contribution from

357 traffic emission and secondary reactions of bio-VOCs also decreased the aromaticity and

358 increased the oxidation degree of HULIS (Liu et al., 2016; Tang et al., 2020). These

359 changes in HULIS compounds led to the decrease in their MAE_{365} values during the haze

360 episode, as described above (Zhong and Jang, 2014; Song et al., 2019).

3.3.1. CHO Compounds

362 The CHO compounds bear O-containing functional groups, and have been

363 frequently detected in ambient aerosols. As shown in Figure 2, the CHO compounds were

364 the predominant component in the four HULIS samples, and the MW_w values for CHO−

365 and CHO+ compounds were 247–288 and 236–272, respectively, with relatively higher

366 MW_w values observed for the CHO group (CHO− and CHO+) in haze HULIS, especially

367 in haze-I samples. This finding may be related to the stronger oxidation of HULIS during

368 haze days, because the aqueous oxidation of biomass burning aerosols was found to yield

369 high MW of organic products (Tomaz et al., 2018; Yu et al., 2016).

370 The OS_C is often used to describe the degree of oxidation of organic species in the

371 atmosphere (Kroll et al., 2011; Wang et al., 2017b). Figure 3 shows plots of OS_C versus

372 carbon number for the CHO compounds. As indicated in the figure, CHO compounds

373 exhibited OS_C from −2 to +1 with up to 40 carbon atoms. Kroll et al. (2011) proposed

374 that compounds with OS_C between −0.5 and +1 and < 18 carbon atoms can be attributed

375 to semi-volatile and low-volatile oxidized organic aerosols (SV-OOA and LV-OOA),

376 which are mainly formed by complex oxidation reactions in atmosphere. Compounds

377 with OS_C between −0.5 and −1.5 and 6–23 carbon atoms are related to primary biomass

378 burning organic aerosol (BBOA). In addition, compounds with OS_C between −1 and −2

379 and ≥18 carbon atoms have been suggested to be hydrocarbon-like organic aerosols

380 (HOA), which are regarded as primary combustion surrogate (Zhang et al., 2005; Kroll et

381 al., 2011; Wang et al., 2017b).

382   As illustrated in Figure 3 and Table S6, most of the CHO− compounds clustered in

383   the BBOA region, accounting for 40%–46% of the total CHO− compounds, thus

384   suggesting that BB may be a major contributor to CHO compounds in HULIS. Figure 3

385   clearly indicates that the majority of aromatic and condensed aromatic compounds

386   produced signals in the OS_C region between −0.5 and 1.0 and carbon number of 3–18

387   (Figure 3), which corresponded to SV-OOA and LV-OOA. The proportions of SV-OOA

388   and LV-OOA accounted for 23%–28% and 1.9%–2.4% of the total CHO− compounds,

389   respectively, and presented no significant variation. In contrast, the HOA components in

390   haze-I days showed the highest abundance (18%), which were much higher than those

391   (3.5%–4.5%) in haze-II, clean-I, and clean-II days. This finding indicated that the

392   increase in the primary source is associated with fossil fuel combustion such as vehicle

393   emissions during the haze bloom period (Zhang et al., 2005).

394   As shown in Figure 3, CHO+ compounds presented lower OS_C (from −2.0 to 1.0)

395   than CHO− compounds. Most of the CHO+ compounds occurred in the BBOA region in

396   all four HULIS samples, making up to 60%–72% of the total CHO+ compounds, which

397   again suggesting that BB is an important contributor to CHO compounds in HULIS. The

398   HOA among CHO+ compounds showed the same changing trends as those among CHO−

399   compounds, and higher HOA abundance was observed during haze-I days. In addition,

400   some high AI_{mod} values of aromatics were found in the regions A1+ and A2+ (Figure 3),

401   which implied that the highest AI_{mod} values (AI ≥ 0.67) with DBE ≥ 22 were only

402   detected during the haze days possibly owing to soot-derived materials or oxidized PAHs

403   (Decesari et al., 2002; Kuang and Shang, 2020). It must be noted that the sampling site in

404   the present study is influenced by traffic sources, the enhanced oxidation of vehicle-

405 exhausted soot also results in the accumulation of water-soluble high aromatic organic

406 species (Decesari et al., 2002).

3.3.2. CHON Compounds

408 In the present study, 1379–2217 and 2008–2943 formulas were assigned to CHON

409 compounds identified in the ESI− and ESI+ spectra, respectively, which accounted for

410 23%–25% (ESI−) and 41%–45% (ESI+) of total identified compounds, respectively.

411 Relatively higher contents of CHON− compounds were obviously detected in HULIS

412 samples obtained during haze-I days, suggesting the occurrence of more N-containing

413 components in HULIS during haze bloom days. As shown in Tables S4 and S5, the

414 average MW_w values for CHON− and CHON+ compounds were 328 and 317 in haze-I

415 days, respectively, which were slightly higher than those determined in haze-II days and

416 all higher than those observed in clean-I and clean-II days. Meanwhile, the $AI_{mod,w}$ values

417 for CHON− in haze days were 0.31–0.34, which were slightly lower than those in clean

418 days (0.37 and 0.40). These findings indicated that more high MW CHON compounds

419 with lower aromatic structures were formed during the haze episode.

420 The O/N_w ratios for CHON− and CHON+ during haze-I and haze-II days were 5.3–

421 5.7 and 3.8, respectively, which were higher than those determined during the two clean

422 periods, confirming that these compounds were highly oxidized during the haze episode

423 (Tables S4 and S5). In general, compounds with O/N ≥ 3 may indicate oxidized N groups

424 such as nitro ($-NO_2$) or nitrooxy ($-ONO_2$), whereas compounds with O/N < 3 may denote

425 the reduced N compounds (i.e., amines) (Lin et al., 2012; Song et al., 2018). In the

426 present study, most of the CHON compounds (79%–91% of CHON– compounds and

427 61%–64% of CHON+ compounds) exhibited O/N ≥ 3, suggesting that high

concentrations of nitro compounds or organonitrates were contained in the CHON compounds. Moreover, these compounds were more abundant in the CHON– group during the haze episode (87%–91%), when compared with those during clean-I and clean-II days (79%–82%), again implying that CHON– compounds undergo relatively higher oxidization during the haze episode. As indicated in Figure 1, the increase in NO_2 was consistent with increased production of highly oxidized N-containing organic compounds (NOCs) during the haze episode, which suggested the significant contribution of NO_3-related multigenerational chemistry to organonitrate aerosol formation (Berkemeier et al., 2016).

The majority of aromatics and condensed aromatics produced clear signals in regions associated with SV-OOA and LV-OOA (Figure 4). BBOA also constituted a significant proportion (33%–39%) in the CHON– group, and a relatively lower BBOA content was observed in haze-I days. The abundance of HOA was relatively lower, accounting for 2.3%–7.8% of the total CHON compounds, and the relative abundance of HOA in haze-I days was much higher than that in haze-II, clean-I, and clean-II days, suggesting the accumulation of primary fossil fuel combustion during haze-I days.

The CHON+ compounds mainly occurred at the range of $-2.0 < OS_C < 1.5$, with average OS_C values of around -1.0 for each sample, clearly indicating that CHON+ compounds were relatively lower than CHON– compounds. Most of the CHON+ compounds were detected in the BBOA region, accounting for 60%–76% of the total $CHON^+$ compounds. The relative contribution of BBOA in haze-I days was lower than that in haze-II and clean days. Moreover, a large number of aromatic species were observed at the region B1+ (Figure 4), demonstrating that higher aromatic compounds

451 were only detected in haze-I days, which may be related to soot or BC. Similar trend was

452 also exhibited by CHO+ compounds, indicating the contribution of local combustion

453 sources (e.g., traffic emission) during haze-I days.

3.3.3. CHOS and CHONS Compounds

455 In this study, 478–696 CHOS compounds and 306–589 CHONS compounds were

456 identified in ESI– mode (Table S4). Among these S-containing compounds, >86% of the

457 CHOS compounds had O/S ratios >4, whereas > 89% of the CHONS compounds

458 presented O/S ratios >7, suggesting that these S-containing compounds were possibly

459 organosulfates and nitrooxyorganosulfates. As listed in Table S4, the $AI_{mod,w}$ values for

460 CHOS and CHONS were about 0.02 and 0.01 in the HULIS fraction, which were much

461 lower than those for CHO and CHON. Almost 99% of the CHOS and CHONS

462 compounds in the HULIS fraction had AI_{mod} values <0.5, while >93% of the CHONS

463 compounds had $AI_{mod} = 0$, indicating that they were mainly comprised of aliphatic and

464 olefinic organosulfates. These results are consistent with the previous findings that the

465 major S-containing compounds among organic aerosols in Guangzhou are organosulfates

466 formed by secondary oxidation reaction of long-chain alkenes/fatty acids with SO_2 (Jiang

467 et al., 2020), which generally possessed long aliphatic carbon chains and a higher degree

468 of oxidation. However, these compounds are different from the S-containing compounds

469 detected during the hazy days in Beijing (Jiang et al., 2016; Mo et al., 2016), which were

470 determined to be aliphatic organosulfates with low degree of oxidation and higher

471 amounts of aromatics and PAH-derived organosulfates, having a strong correlation with

472 anthropogenic emissions.

473   As described earlier, CHOS− and CHONS− compounds might be related to

474   organosulfates or nitrooxyorganosulfates, which have been observed to be derived from

475   atmospheric reactions of bio-VOCs such as α-pinene, limonene, and isoprene (Huang et

476   al., 2018; Surratt *et al.*, 2008) and fossil fuel combustion including coal combustion, off-

477   road engine emissions (Song et al., 2018, 2019; Cui et al., 2019). In the present study, the

478   relative contents of S-containing compounds (CHOS+CHONS) in the HULIS fraction in

479   haze days were all higher than those in clean days (Figure 2). Moreover, the CHOS and

480   CHONS compounds in haze HULIS always have relatively high relatively O/S ratios

481   than those in clean HULIS. These findings suggested the relatively higher contribution of

482   SO_2-related chemical oxidation during the haze event.

483   **3.3.4. CHN Compounds**

484   The N-bases (CHN) are usually identified in ambient aerosols and smokes from BB.

485   In the present study, 110–165 CHN+ compounds were identified in ESI+ mode, with

486   most of them (>86%) presenting DBE ≥ 2, suggesting that they might be nitrile and

487   amine species (Lin et al., 2012). As shown in Figure 2, the abundances of CHN+

488   compounds were 2.0%–3.6% in the haze days, which were much higher than those noted

489   in clean days (1.3%–1.4%), indicating higher contribution of CHN+ compounds to the

490   HULIS fraction during the haze episode. The MW_w values for CHN+ compounds were

491   204–223, which were lower than those for the other groups (i.e., CHO+, CHON+) (Table

492   S5). However, the average AI_{mod} values for N-bases (0.37–0.48) detected in the ESI+

493   mode were much higher than those for CHO+ (0.11–0.12) and CHON+ (0.20–0.22)

494   compounds, implying that these reduced CHN+ compounds exhibited more unsaturated

495   or aromatic structures.

496   To further understand the molecular distribution of CHN+ compounds during the

497   haze process, van Krevelen (VK) diagrams were constructed by plotting the H/C ratio

498   versus N/C ratio (Figure S2). It was obvious that this plot could separate the compound

499   classes with different degree of AI. As shown in Figure S2, compounds (denoted in black

500   color) in the upper region of the VK diagram had one N atom with DBE = 0, indicating

501   that they are aliphatic amines. It can be noted from Table S7 that the aliphatic group

502   presented the lowest abundance in all the samples, suggesting that the CHN+ compounds

503   possessed comparatively lower aliphatic structures. Olefinic compounds showed the

504   highest abundance in the four samples, which accounted for 37%–51% of the total CHN+

505   compounds. Importantly, a large proportion of the compounds (>39%) exhibited high

506   degree of AI (AI > 0.5) (Figure S2 and Table S7), suggesting a large amounts of aromatic

507   structure and N-heterocyclic ring in HULIS. Moreover, the CHN+ compounds in haze-I

508   days presented obviously lower content of aromatic structures than those in haze-II,

509   clean-I, and clean-II days, signifying the relatively high contribution of fossil fuel

510   combustion (which generally emits more low-aromatic CHN compounds) during the haze

511   bloom episode(Song et al., 2022). In addition, the CHN+ group also constituted a large

512   proportion of BBOA (Table S6), which indicated the significant contribution of BB.

513   However, it must be noted that a relatively lower content of BBOA was detected during

514   haze-I days, which was consistent with the changing trends of CHON- or CHON+

515   compounds during the haze episode. These results suggested the relatively lower

516   contribution of BB during haze-I days, because quiet and stable weather conditions can

517   prevent regional transport of BB sources during this stage (Wu et al., 2018).

3.4. Factors influencing light absorption and molecular characteristics of HULIS

during the haze bloom-decay process

As described earlier, the light absorption properties of HULIS exhibited obvious variation during the haze bloom-decay process. The average Abs_{365} value for HULIS was 0.55 ± 0.06 M m^{-1} in clean-I days, which first increased to 3.4 ± 1.5 M m^{-1} in haze-I days, then slowly decreased to 2.6 ± 0.85 M m^{-1} in haze-II days, and finally rapidly declined to 0.64 ± 0.32 M m^{-1} in clean-II days. In general, the light absorption of HULIS can be related to their chemical and molecular properties that are influenced by factors such as sources, secondary formation, and aging process. The results of principal component analysis (PCA) obviously showed a positive loading for principal component 1 (PC1), and the Abs_{365} values for HULIS were clustered with EC, K_{bb}^+, Lev, NH_4^+, and NO_3^- (Figure 5). These results suggested that BB and other sources such as new particle formation could contribute to light absorption of HULIS (An et al., 2019; Song et al., 2019). Similarly, the findings of Pearson correlation coefficient analysis revealed that the Abs_{365} values for HULIS exhibited significant positive correlations with K_{bb}^+ ($r = 0.728$, $p < 0.01$) and Lev ($r = 0.800$, $p < 0.01$) (Table S8). As Lev and K_{bb}^+ are generally considered as tracers derived from BB, these results suggested the significant contribution of BB to light absorption of HULIS. This observation was also supported by the abundance of BBOA compounds detected in all the four HULIS samples (Table S6). The significant positive relationships between the Abs_{365} values for HULIS and secondary ions (i.e., NO_3^- ($r = 0.702$, $p < 0.01$), SO_4^{2-} ($r = 0.554$, $p < 0.05$), and NH_4^+ ($r = 0.899$, $p < 0.01$)) indicated the important impact of secondary formation on the light absorption of HULIS. Besides, the Abs_{365} values for HULIS were also strongly correlated

541   with NO_2, O_3, and NO_2, which confirmed the important impact of atmospheric oxidation

542   reactions on the light absorption of HULIS.

543   It must be noted that MAE_{365} is a key parameter signifying the light absorption

544   ability of HULIS. As listed in Table S2, the MAE_{365} values for HULIS varied in different

545   stages, and were lower in haze days owing to the variation in the chemical and molecular

546   composition of HULIS during the haze bloom-decay process. Furthermore, the AI_{mod}

547   values for HULIS varied in different stages (Tables S4), and were relatively lower in

548   haze days, indicating that haze HULIS have comparatively lower degree of conjugation

549   or aromaticity. This finding suggested that the HULIS compounds may undergo higher

550   oxidation during the haze episode, causing a decline in chromophores and reduction in

551   the light absorption capacity of HULIS (Lin et al., 2017). Besides, the accumulated

552   contribution of organic compounds from vehicle emission and secondary chemical

553   reactions of bio-VOCs may also dilute light-absorbing compounds in haze HULIS (Tang

554   et al., 2020; Liu et al., 2016).

555   Lin et al. (2018) reported that potential light-absorbing chromophores can be

556   determined in the region between $DBE = 0.5 \times C$ (linear conjugated polyenes $C_xH_yC_2$)

557   and $DBE = 0.9 \times C$ (fullerene-like hydrocarbons). In the present study, most of the high-

558   intensity CHON, CHO, and CHN compounds with high AI values were clustered in

559   potential BrC chromophore region (Figures S3 and S4), which mainly comprised CHON

560   (46%–50% in ESI- mode and 56%–62% in ESI+ mode, respectively) and CHO (44%–48%

561   in ESI- mode and 29%–38% in ESI+ mode, respectively) compounds (Table 1).

562   Although the contribution of CHN+ compounds to BrC was relatively lower, the content

563   of potential chromophores among the total CHN+ compounds was higher than those in

564   CHON+ and CHO+ compounds. Therefore, these three groups of light-absorbing

565   compounds (i.e., CHON+, CHN+, and CHO+ compounds) were further examined. As

566   shown in Table 1, the Int_C/Int_{BrC} values of CHO− (i.e., content of CHO− chromophores

567   in the total chromophores) decreased from 48% to 44% whereas the Int_C/Int_{BrC} values of

568   CHON− increased from 46% to 50% during the haze bloom process. These findings

569   indicated that more NOCs chromophores were formed during this stage in which higher

570   NO_2 concentration may be preferred for the formation of N-containing chromophores

571   such as nitrophenols. However, it must be noted that the proportions of both CHO− and

572   CHON− chromophores among the total identified compounds decreased from clean-I to

573   haze-I days, suggesting the occurrence of stronger photo-bleaching process during the

574   haze bloom stage (Zeng et al., 2020). Likewise, both CHO+ and CHON+ compounds

575   presented similar variation during the entire study period. In addition, the CHN+

576   compounds also exhibited higher Int_C/Int_{BrC} values during the haze bloom process and

577   suggesting the accumulated contribution from local combustion process. Furthermore, the

578   proportion of CHON+ chromophores in the total CHON+ compounds increased with the

579   decreasing content of CHN+ chromophores, may implying that some aromatic CHN

580   compounds were transformed to CHON+ compounds during the aging process.

581

4. Conclusions

583   This study investigated the evolution of light absorption and molecular properties of

584   HULIS during a winter haze bloom-decay process, and examined the key factors

585   affecting the light absorption of HULIS in Guangzhou, China. The results showed that

586   HULIS exhibited significant variation in light absorption during the haze bloom-decay

process. First, higher Abs_{365} values were observed in haze days, indicating the presence of significant amounts of light-absorbing organic compounds during the haze episode. However, the MAE_{365} values for HULIS in haze days were relatively lower than those in clean days, suggesting the light absorption capabilities of HULIS were weakened during the haze event. Furthermore, CHON and CHO compounds, exhibiting relatively higher degree of conjugated structure, were the most abundant groups in all the HULIS samples, and were also the major contributors to light absorption capacity of HULIS. Importantly, the molecular properties of HULIS dynamically varied during the entire haze episode. When compared with HULIS in clean days, those in haze days presented relatively lower AI_{mod} values and higher O/C_w, O/N_w, and O/S_w ratios, suggesting the predominance of compounds with low aromaticity and higher oxidation in HULIS during haze episode. These results indicated that HULIS compounds undergo relatively stronger oxidation during the haze days. Moreover, PCA and Pearson correlation analysis revealed that BB and secondary chemical formation both contributed to the variation in the light absorption properties of HULIS. Both primary sources (such as accumulated contribution of organic compounds formed from local traffic emission) and secondary sources (such as stronger chemical reactions) led to the rapid increase in HULIS during the haze bloom days. However, stronger oxidation of HULIS compounds were observed during the haze episode, and some potential BrC chromophores were degraded. In addition, the chemical reactions of bio-VOCs such as isoprene also diluted the light-absorbing compounds in HULIS.

Thus, the present study provides novel insights into the light and molecular evolution of HULIS during haze event, which are important for predicting the

environmental and climatic effects of HULIS. However, as this study examined only one haze bloom-decay process in winter in Guangzhou, the results obtained may be not adequate for understanding all the haze episodes in South China. Therefore, there is a need for a comprehensive investigation of haze episode in different seasons and regions in future.

Data availability

The research data are available in the Harvard Dataverse (https://doi.org/10.7910/DVN/DYGYQT, Song, 2022).

Author contributions. J. Song and P. Peng designed the research together. C, Zou, T. Cao, and M. Li carried out the $PM_{2.5}$ sampling experiments. C, Zou and T. Cao extracted and analyzed the WSOC and HULIS samples. B. Jiang analyzed the HULIS samples by FT-ICR MS. C. Zou and J. Song wrote the paper. J. Li, X. Ding, Z Yu, and G. Zhang commented and revised the paper.

Competing interests. The authors declare that they have no conflict of interest

Acknowledgments. This study was supported by the National Natural Science Foundation of China (42192514 and 41977188), Guangdong Foundation for Program of Science and Technology Research (2020B1212060053), and Guangdong Foundation for Program of Science and Technology Research (2019B121205006).

References

An, Z., Huang, R. J., Zhang, R., Tie, X., Li, G., Cao, J., Zhou, W., Shi, Z., Han, Y., Gu, Z., and Ji, Y.: Severe haze in northern China: A synergy of anthropogenic emissions and atmospheric processes, Proc Natl Acad Sci USA, 116, 8657-8666, 10.1073/pnas.1900125116, 2019.

Berkemeier, T., Ammann, M., Mentel, T. F., Poschl, U., and Shiraiwa, M.: Organic nitrate contribution to new particle formation and growth in secondary organic aerosols from alpha-pinene ozonolysis, Environ Sci Technol, 50, 6334-6342, 10.1021/acs.est.6b00961, 2016.

Bianco, A., Deguillaume, L., Vaitilingom, M., Nicol, E., Baray, J. L., Chaumerliac, N., and Bridoux, M.: Molecular characterization of cloud water samples collected at the Puy de Dome (France) by Fourier transform ion cyclotron resonance mass spectrometry, Environ Sci Technol, 52, 10275-10285, doi:10.1021/acs.est.8b01964, 2018.

Cao, T., Li, M., Zou, C., Fan, X., Song, J., Jia, W., Yu, C., Yu, Z., Peng, P.: Chemical composition, optical properties, and oxidative potential of water-and methanol-soluble organic compounds emitted from the combustion of biomass materials and coal, Atmos Chem Phys, 21, 13187-13205, doi: 10.5194/acp-21-13187-2021, 2021.

Chen, Q., Ikemori, F., Mochida, M.: Light absorption and excitation-emission fluorescence of urban organic aerosol components and their relationship to chemical structure, Environ. Sci. Technol., 50, 10859-10868, doi: 10.1021/acs.est.6b02541, 2016.

Cui, M., Li, C., Chen, Y. J., Zhang, F., Li, J., Jiang, B., Mo, Y., Li, J., Yan, C., Zheng, M., Xie, Z., Zhang, G., and Zheng, J.: Molecular characterization of polar organic aerosol constituents in off-road engine emissions using Fourier transform ion cyclotron resonance mass spectrometry (FT-ICR MS): implications for source apportionment, Atmos Chem Phys, 19, 13945-13956, doi:10.5194/acp-19-13945-2019, 2019.

Dasari, S., Andersson, A., Bikkina, S., Holmstrand, H., Budhavant, K., Satheesh, S., Asmi, E., Kesti, J., Backman, J., Salam, A., Bisht, D. S., Tiwari, S., Hameed, Z., and Gustafsson, Ö.: Photochemical degradation affects the light absorption of water-soluble brown carbon in the South Asian outflow, Sci Adv, 5, eaau8066, doi: 10.1126/sciadv.aau8066, 2019.

Decesari, S., Facchini, M. C., Matta, E., Mircea, M., Fuzzi, S., Chughtai, A. R., and Smith, D. M.: Water soluble organic compounds formed by oxidation of soot, Atmos Environ, 36, 1827-1832, 10.1016/s1352-2310(02)00141-3, 2002.

Deng, J., Ma, H., Wang, X., Zhong, S., Zhang, Z., Zhu, J., Fan, Y., Hu, W., Wu, L., Li, X., Ren, L., Pavuluri, C.M., Pan, X., Sun, Y., Wang, Z., Kawamura, K., and Fu, P.: Measurement report: Optical properties and sources of water-soluble brown carbon in Tianjin, North China –insights from organic molecular compositions, Atmos. Chem. Phys., 22, 6449–6470, doi: 10.5194/acp-22-6449-2022, 2022.

Du, Z., He, K., Cheng, Y., Duan, F., Ma, Y., Liu, J., Zhang, X., Zheng, M., and Weber, R.: A yearlong study of water-soluble organic carbon in Beijing II: Light absorption properties, Atmos Environ, 89, 235-241, 10.1016/j.atmosenv.2014.02.022, 2014.

Fan, X. J., Song, J. Z., and Peng, P. A.: Comparison of isolation and quantification methods to measure humic-like substances (HULIS) in atmospheric particles, Atmos. Environ., 60, 366–374, 10.1016/j.atmosenv.2012.06.063, 2012.

Fan, X., Song, J., Peng, P.: Comparative study for separation of atmospheric humiclike substance (HULIS) by ENVI-18, HLB, XAD-8 and DEAE sorbents: elemental composition, FT-IR, 1H-NMR and off-line thermochemolysis with tetramethylammonium hydroxide (TMAH). Chemosphere 93, 1710–1719, 10.1016/j.chemosphere.2013.05.045, 2013.

Fan, X., Song, J., and Peng, P.: Temporal variations of the abundance and optical properties of water soluble Humic-Like Substances (HULIS) in $PM_{2.5}$ at Guangzhou, China, Atmos Res, 172-173, 8-15, doi:10.1016/j.atmosres.2015.12.024, 2016.

Fan, X., Cao, T., Yu, X., Wang, Y., Xiao, X., Li, F., Xie, Y., Ji, W., Song, J., and Peng, P: The evolutionary behavior of chromophoric brown carbon during ozone aging of fine particles from biomass burning, Atmos Chem Phys, 20, 4593-4605, doi:10.5194/acp-20-4593-2020, 2020.

Forrister, H., Liu, J., Scheuer, E., Dibb, J., Ziemba, L., Thornhill, K. L., Anderson, B., Diskin, G., Perring, A. E., Schwarz, P., Campuzano-Jost, P., Day, D. A., Palm, B. B., Jimenez, J. L., Nenes, A., and Weber, R. J.: Evolution of brown carbon in wildfire plumes, Geophys. Res. Lett., 42, 4623–4630, doi: 10.1002/2015gl063897, 2015.

Graber and Rudich: Atmospheric HULIS: How humic-like are they? A comprehensive and critical review, Atmos Chem Phys, 6, 729-753, 2006.

Huang, R. J., Yang, L., Cao, J., Chen, Y., Chen, Q., Chen, Q., Li, Y. J., Duan, J., Zhu, C. C., Dai, W. T., Wang, K., Lin, C. S.;,Ni, H. Y., Corbin, J. C., Wu, Y. F., Zhang, R. J.

Tie, X. X., Hoffmann, T., O'Dowd, C., and Dusek, U.: Brown carbon aerosol in urban Xi'an, Northwest China: The composition and light absorption properties, Environ Sci Technol, 52, 6825-6833, doi:10.1021/acs.est.8b02386, 2018.

Huang, R. J., Yang, L., Shen, J. C., Yuan, W., Gong, Y. Q., Guo, J., Cao, W., Duan, J., Ni, H., Zhu, C., Dai, W., Li, Y., Chen, Y., Chen, Q., Wu, Y., Zhang, R., Dusek, U., O'Dowd, C., and Hoffmann, T.: Water-insoluble organics dominate brown carbon in wintertime urban aerosol of China: chemical characteristics and optical properties, Environ Sci Technol, 54, 7836-7847, doi:10.1021/acs.est.0c01149, 2020.

Jiang, B., Kuang, B. Y., Liang, Y., Zhang, J., Huang, X. H. H., Xu, C., Yu, J. Z., and Shi, Q.: Molecular composition of urban organic aerosols on clear and hazy days in Beijing: a comparative study using FT-ICR MS, Environ. Chem., 13, 888–901, https://doi.org/10.1071/en15230, 2016.

Jiang, H., Li, J., Chen, D., Tang, J., Cheng, Z., Mo, Y., Su, T., Tian, C., Jiang, B., Liao, Y., and Zhang, G.: Biomass burning organic aerosols significantly influence the light absorption properties of polarity-dependent organic compounds in the Pearl River Delta Region, China, Environ Int, 144, 106079, 10.1016/j.envint.2020.106079, 2020.

Jiang, H., Li, J., Sun, R., Liu, G., Tian, C., et al. Determining the sources and transport of brown carbon using radionuclide tracers and modeling, J Geophys Res Atmos, 126, e2021JD034616, doi:org/10.1029/2021JD034616, 2021.

Kampf, C. J., Filippi, A., Zuth, C., Hoffmann, T., and Opatz, T.: Secondary brown carbon formation via the dicarbonyl imine pathway: nitrogen heterocycle formation and synergistic effects, Phys Chem Chem Phys, 18, 18353-18364, 10.1039/c6cp03029g, 2016.

723   Kroll, J. H., Donahue, N. M., Jimenez, J. L., Kessler, S. H., Canagaratna, M. R., Wilson,

724   K. R., Altieri, K. E., Mazzoleni, L. R., Wozniak, A. S., Bluhm, H., Mysak, E. R.,

725   Smith, J. D., Kolb, C. E., and Worsnop, D. R.: Carbon oxidation state as a metric for

726   describing the chemistry of atmospheric organic aerosol, Nature Chem, 3, 133-139,

727   10.1038/nchem.948, 2011.

728   Kuang, K. and Shang, J.: Changes in light absorption by brown carbon in soot particles

729   due to heterogeneous ozone aging in a smog chamber, Environ Pollut, 266, 115273,

730   10.1016/j.envpol.2020.115273, 2020.

731   Laskin, A., Laskin, J., and Nizkorodov, S. A.: Chemistry of atmospheric brown carbon,

732   Chem Rev, 115, 4335-4382, 10.1021/cr5006167, 2015.

733   Li, K., Jacob, D. J., Liao, H., Shen, L., Zhang, Q., and Bates, K.H.: Anthropogenic

734   drivers of 2013–2017 trends in summer surface ozone in China, Proc Natl Acad Sci

735   USA, 116, 422–427, https://doi.org/10.1073/pnas.1812168116, 2019.

736   Li, M., Fan, X., Zhu, M., Zou, C., Song, J., Wei, S., Jia, W., and Peng, P.: Abundance

737   and light absorption properties of brown carbon emitted from residential coal

738   combustion in China, Environ Sci Technol, 53, 595-603,

739   doi:10.1021/acs.est.8b05630, 2019.

740   Li, S. W., Chang, M., Li, H., Cui, X. Y., and Ma, L. Q.: Chemical compositions and

741   source apportionment of $PM_{2.5}$ during clear and hazy days: seasonal changes and

742   impacts of Youth Olympic Games, Chemosphere, 256, 127163,

743   10.1016/j.chemosphere.2020.127163, 2020.

Li, P. and Hur, J., Utilization of UV-Vis spectroscopy and related data analyses for dissolved organic matter (DOM) studies: A review, Crit. Rev. Environ. Sci. Technol., 47, 131–154, doi: 10.1080/10643389.2017.1309186, 2017.

Lin, P.; Engling, G.; Yu, J. Z.: Humic-like substances in fresh emissions of rice straw burning and in ambient aerosols in the Pearl River Delta Region, China. Atmos Chem Phys, 10, 6487−6500, 10.5194/acp-10-6487-2010, 2010.

Lin, P., Bluvshtein, N., Rudich, Y., Nizkorodov, S. A., Laskin, J., and Laskin, A.: Molecular chemistry of atmospheric brown carbon inferred from a nationwide biomass burning event, Environ Sci Technol, 51, 11561-11570, 10.1021/acs.est.7b02276, 2017.

Lin, P., Rincon, A. G., Kalberer, M., and Yu, J. Z.: Elemental composition of HULIS in the Pearl River Delta Region, China: results inferred from positive and negative electrospray high resolution mass spectrometric data, Environ Sci Technol, 46, 7454-7462, 10.1021/es300285d, 2012.

Lin, P., Fleming, L. T., Nizkorodov, S. A., Laskin, J., and Laskin,A.: Comprehensive molecular characterization of atmospheric brown carbon by high resolution mass spectrometry with electrospray and atmospheric pressure photoionization, Anal Chem, 90, 12493-12502. doi:10.1021/acs.analchem.8b02177, 2018.

Liu, J., Lin, P., Laskin, A., Laskin, J., Kathmann, S. M., Wise, M., Caylor, R., Imholt, F., Selimovic, V., and Shilling, J. E.: Optical properties and aging of light-absorbing secondary organic aerosol, Atmos Chem Phys, 16, 12815-12827, 10.5194/acp-16-12815-2016, 2016.

766   Liu, J., Mo, Y., Ding, P., Li, J., Shen, C., and Zhang, G.: Dual carbon isotopes ((14)C

767   and (13)C) and optical properties of WSOC and HULIS-C during winter in

768   Guangzhou,   China,   Sci   Total   Environ,   633,   1571-1578,

769   10.1016/j.scitotenv.2018.03.293, 2018.

770   Ma, Y., Cheng, Y., Qiu, X., Cao, G., Kuang, B., Yu, J. Z., and Hu, D.: Optical properties,

771   source apportionment and redox activity of humic-like substances (HULIS) in

772   airborne fine particulates in Hong Kong, Environ Pollut, 255, 113087,

773   10.1016/j.envpol.2019.113087, 2019.

774   Mo, Y., Li, J., Jiang, B., Su, T., Geng, X., Liu, J., Jiang, H., Shen, C., Ding, P., Zhong, G.,

775   Cheng, Z., Liao, Y., Tian, C., Chen, Y., and Zhang, G.: Sources, compositions, and

776   optical properties of humic-like substances in Beijing during the 2014 APEC summit:

777   Results from dual carbon isotope and Fourier-transform ion cyclotron resonance

778   mass   spectrometry   analyses,   Environ   Pollut,   239,   322-331,

779   10.1016/j.envpol.2018.04.041, 2018.

780   Mohr, C., Lopez-Hilfiker, F. D., Zotter, P., Prevot, A. S., Xu, L., Ng, N. L., Herndon, S.

781   C., Williams, L. R., Franklin, J. P., Zahniser, M. S., Worsnop, D. R., Knighton, W.

782   B., Aiken, A. C., Gorkowski, K. J., Dubey, M. K., Allan, J. D., and Thornton, J. A.:

783   Contribution of nitrated phenols to wood burning brown carbon light absorption in

784   Detling, United Kingdom during winter time, Environ Sci Technol, 47, 6316-6324,

785   10.1021/es400683v, 2013.

786   Ni, H., Huang, R. J., Pieber, S. M., Corbin, J. C., Stefenelli, G., Pospisilova, V., Klein, F.,

787   Gysel-Beer, M., Yang, L., Baltensperger, U., Haddad, I. E., Slowik, J. G., Cao, J.,

Prevot, A. S. H., and Dusek, U.: Brown carbon in primary and aged coa lcombustion emission, Environ Sci Technol, 55, 5701-5710, 10.1021/acs.est.0c08084, 2021.

Park, S., Yua, G.-H., and Lee, S., Optical absorption characteristics of brown carbon aerosols during the KORUS-AQ campaign at an urban site, Atmos. Res., 203, 16–27, doi: 10.1016/j.atmosres.2017.12.002, 2018.

Saleh, R., Hennigan, C. J., McMeeking, G. R., Chuang, W. K., Robinson, E. S., Coe, H., Donahue, N. M., and Robinson, A. L.: Absorptivity of brown carbon in fresh and photo-chemically aged biomass-burning emissions, Atmos. Chem. Phys., 13, 7683–7693, doi: 10.5194/acp-13-7683-2013, 2013.

Shen, Z., Zhang, Q., Cao, J., Zhang, L., Lei, Y., Huang, Y., Huang, R. J., Gao, J., Zhao, Z., Zhu, C., Yin, X., Zheng, C., Xu, H., and Liu, S.: Optical properties and possible sources of brown carbon in PM 2.5 over Xi'an, China, Atmos Environ, 150, 322-330, 10.1016/j.atmosenv.2016.11.024, 2017.

Song, J.: Data for SJ, Harvard Dataverse [data set], (https://doi.org/10.7910/DVN/DYGYQT, 2022.

Song, J. Z., Li, M. J., Fan, X. J., Zou, C. L., Zhu, M. B., Jiang, B., Yu, Z. Q., Jia, W. L., Liao, Y. H., and Peng, P. A.: Molecular characterization of water- and methanol-soluble organic compounds emitted from residential coal combustion using ultrahigh-resolution electrospray ionization Fourier transform ion cyclotron resonance mass spectrometry, Environ Sci Technol, 53, 13607-13617, 10.1021/acs.est.9b04331, 2019.

Song, J. Z., Li, M. J., Jiang, B., Wei, S. Y., Fan, X. J., and Peng, P. A.: Molecular Characterization of Water-Soluble Humic like substances in smoke particles emitted

from combustion of biomass materials and coal using ultrahigh-resolution electrospray ionization Fourier transform ion cyclotron resonance mass spectrometry, Environ Sci Technol, 52, 2575-2585, 10.1021/acs.est.7b06126, 2018.

Song, J. Z., Li, M. J., Zou, C. L., Cao, T., Fan, X. J., Jiang, B., Yu, Z. Q., Jia, W. L., and Peng, P. A.: Molecular characterization of nitrogen-containing compounds in humic-like substances emitted from biomass burning and coal combustion, Environ Sci Technol, 56, 119-130, doi:10.1021/acs.est.1c04451, 2022.

Sumlin, B. J., Pandey, A., Walker, M. J., Pattison, R. S., Williams, B. J., and Chakrabarty, R. K.: Atmospheric photooxidation diminishes light absorption by primary brown carbon aerosol from biomass burning, Environ Sci Tech Let, 4, 540-545, 10.1021/acs.estlett.7b00393, 2017.

Surratt, J. D., Gomez-Gonzalez, Y., Chan, A. W. H., Vermeylen, R., Shahgholi, M., Kleindienst, T. E., Edney, E. O., Offenberg, J. H., Lewandowski, M., Jaoui, M., Maenhaut, W., Claeys, M., Flagan, R. C., and Seinfeld, J. H.: Organosulfate formation in biogenic secondary organic aerosol, J Phys Chem A, 112, 8345-8378, 10.1021/jp802310p, 2008.

Tan, J., Xiang, P., Zhou, X., Duan, J., Ma, Y., He, K., Cheng, Y., Yu, J., and Querol, X.: Chemical characterization of humic-like substances (HULIS) in $PM_{2.5}$ in Lanzhou, China, Sci Total Environ, 573, 1481-1490, 10.1016/j.scitotenv.2016.08.025, 2016.

Tang, J., Li, J., Su, T., Han, Y., Mo, Y. Z., Jiang, H. X., Cui, M., Jiang, B., Chen, Y. J., Tang, J. H., Song, J. Z., Peng, P. A., and Zhang, G.: Molecular compositions and optical properties of dissolved brown carbon in biomass burning, coal combustion, and vehicle emission aerosols illuminated by excitation-emission matrix

834   spectroscopy and Fourier transform ion cyclotron resonance mass spectrometry

835   analysis, Atmos Chem Phys, 20, 2513-2532, 10.5194/acp-20-2513-2020, 2020.

836   Tomaz, S., Cui, T., Chen, Y., Sexton, K. G., Roberts, J. M., Warneke, C., Yokelson, R. J.,

837   Surratt, J. D., and Turpin, B. J.: Photochemical Cloud Processing of primary wildfire

838   emissions as a ptential source of secondary organic Aerosol, Environ Sci Technol, 52,

839   11027-11037, 10.1021/acs.est.8b03293, 2018.

840   Wang, J., Wang, G., Gao, J., Wang, H., Ren, Y., Li, J., Zhou, B., Wu, C., Zhang, L.,

841   Wang, S., and Chai, F.: Concentrations and stable carbon isotope compositions of

842   oxalic acid and related SOA in Beijing before, during, and after the 2014 APEC,

843   Atmos Chem Phys, 17, 981-992, 10.5194/acp-17-981-2017, 2017a.

844   Wang, X. K., Hayeck, N., Bruggemann, M., Yao, L., Chen, H. F., Zhang, C., Emmelin,

845   C., Chen, J. M., George, C., and Wang, L.: Chemical characteristics of organic

846   aerosols in shanghai: a study by ultrahigh-performance liquid chromatography

847   coupled with orbitrap mass spectrometry, J Geophy Res Atmos, 122, 11703-11722,

848   10.1002/2017jd026930, 2017b.

849   Wang, Y., Hu, M., Lin, P., Tan, T., Li, M., Xu, N., Zheng, J., Du, Z., Qin, Y., Wu, Y., Lu,

850   S., Song, Y., Wu, Z., Guo, S., Zeng, L., Huang, X., and He, L.: Enhancement in

851   particulate organic nitrogen and light absorption of humic-like substances over

852   Tibetan Plateau due to long-range transported biomass burning emissions, Environ

853   Sci Technol, 53, 14222-14232, 10.1021/acs.est.9b06152, 2019.

854   Wang, X., Hayeck, N., Brüggemann, M., Abis, L., Riva, M., Lu, Y., Wang, B., Chen, J.,

855   George, C., and Wang, L.: Chemical characteristics and brown carbon chromophores

of atmospheric organic aerosols over the Yangtze River channel: a cruise campaign, J Geophy Res Atmos, 125, 10.1029/2020jd032497, 2020.

Wong, J. P. S., Nenes, A., and Weber, R. J.: Changes in Light Absorptivity of Molecular Weight Separated Brown Carbon Due to Photolytic Aging, Environ Sci Technol, 51, 8414-8421, 10.1021/acs.est.7b01739, 2017.

Wu, Z., Wang, Y., Tan, T., Zhu, Y., Li, M., Shang, D., Wang, H., Lu, K., Guo, S., Zeng, L., and Zhang, Y.: Aerosol liquid water driven by anthropogenic inorganic salts: implying its key role in haze formation over the North China Plain, Environ Sci Technol Lett, 5, 160-166, 10.1021/acs.estlett.8b00021, 2018.

Yang, X., Lu, K., Ma, X., Gao, Y., Tan, Z., Wang, H., Chen, X., Li, X., Huang, X., He, L., Tang, M., Zhu, B., Chen, S., Dong, H., Zeng, L., and Zhang, Y.: Radical chemistry in the Pearl River Delta: observations and modeling of OH and HO_2 radicals in Shenzhen in 2018. Atmos Chem Phys, 22, 12525-12542, 10.5194/acp-22-12525-2022, 2022.

Yu, L., Smith, J., Laskin, A., George, K. M., Anastasio, C., Laskin, J., Dillner, A. M., and Zhang, Q.: Molecular transformations of phenolic SOA during photochemical aging in the aqueous phase: competition among oligomerization, functionalization, and fragmentation, Atmos Chem Phys, 16, 4511-4527, 10.5194/acp-16-4511-2016, 2016.

Yu, X., Yu, Q., Zhu, M., Tang, M., Li, S., Yang, W., Zhang, Y., Deng, W., Li, G., Yu, Y., Huang, Z., Song, W., Ding, X., Hu, Q., Li, J., Bi, X., and Wang, X.: Water soluble organic nitrogen (WSON) in ambient fine particles over a megacity in South China:

spatiotemporal variations and source apportionment, J Geophy Res Atmos, 122, 10.1002/2017jd027327, 2017.

Yuan, W., Huang, R. J., Yang, L., Ni, H., Wang, T., Cao, W., Duan, J., Guo, J., Huang, H., and Hoffmann, T.: Concentrations, optical properties and sources of humic-like substances (HULIS) in fine particulate matter in Xi'an, Northwest China, Sci Total Environ, 789, 147902, 10.1016/j.scitotenv.2021.147902, 2021.

Zeng, Y., Shen, Z., Takahama, S., Zhang, L., Zhang, T., Lei, Y., Zhang, Q., Xu, H., Ning, Y., Huang, Y., Cao, J., and Rudolf, H.: Molecular Absorption and Evolution Mechanisms of PM 2.5 Brown carbon revealed by electrospray ionization Fourier transform–ion cyclotron resonance mass spectrometry during a severe winter pollution episode in Xi'an, China, Geophy Res Lett, 47, 10.1029/2020gl087977, 2020.

Zhan, Y., Li, J., Tsona, N.T., Chen, B., Yan, C., George, C., and Du, L.: Seasonal variation of water-soluble brown carbon in Qingdao, China: Impacts from marine and terrestrial emissions, Environ. Res., 212, 113144, doi: 10.1016/j.envres.2022.113144, 2022.

Zhang, J., Liu, L., Xu, L., Lin, Q., Zhao, H., Wang, Z., Guo, S., Hu, M., Liu, D., Shi, Z., Huang, D., and Li, W.: Exploring wintertime regional haze in northeast China: role of coal and biomass burning, Atmos Chem Phys, 20, 5355-5372, 10.5194/acp-20-5355-2020, 2020.

Zhang, L., Wang, G., Wang, J., Wu, C., Cao, C., and Li, J.: Chemical composition of fine particulate matter and optical properties of brown carbon before and during heating season in Xi'an, Journal of Earth Environment, 8, 451-458, 2017.

901 Zhang, Q., Worsnop, D. R., Canagaratna, M. R., and Jimenez, J. L.: Hydrocarbon-like

902   and oxygenated organic aerosols in Pittsburgh: insights into sources and processes of

903   organic aerosols, Atmos Chem Phys, 5, 3289-3311, 10.5194/acp-5-3289-2005, 2005.

904 Zhang, Y.-L., El-Haddad, I., Huang, R.-J., Ho, K.-F., Cao, J.-J., Han, Y., Zotter, P.,

905   Bozzetti, C., Daellenbach, K. R., Slowik, J. G., Salazar, G., Prévôt, A. S. H., and

906   Szidat, S.: Large contribution of fossil fuel derived secondary organic carbon to water

907   soluble organic aerosols in winter haze in China, Atmos Chem Phys, 18, 4005-4017,

908   10.5194/acp-18-4005-2018, 2018.

909 Zhong, M. and Jang, M.: Dynamic light absorption of biomass-burning organic carbon

910   photochemically aged under natural sunlight, Atmos Chem Phys, 14, 1517-1525,

911   10.5194/acp-14-1517-2014, 2014.

912 Zhu, C. S., Cao, J. J., Huang, R. J., Shen, Z. X., Wang, Q. Y., and Zhang, N. N.: Light

913   absorption properties of brown carbon over the southeastern Tibetan Plateau, Sci

914   Total Environ, 625, 246-251, 10.1016/j.scitotenv.2017.12.183, 2018.

915 Zou, C., Li, M., Cao, T., Zhu, M., Fan, X., Peng, S., Song, J., Jiang, B., Jia, W., Yu, C.,

916   Song, H., Yu, Z., Li, J., Zhang, G., and Peng, P. a.: Comparison of solid phase

917   extraction methods for the measurement of humic-like substances (HULIS) in

918   atmospheric particles, Atmos Environ, 225, 117370,

919   10.1016/j.atmosenv.2020.117370, 2020.

920

921
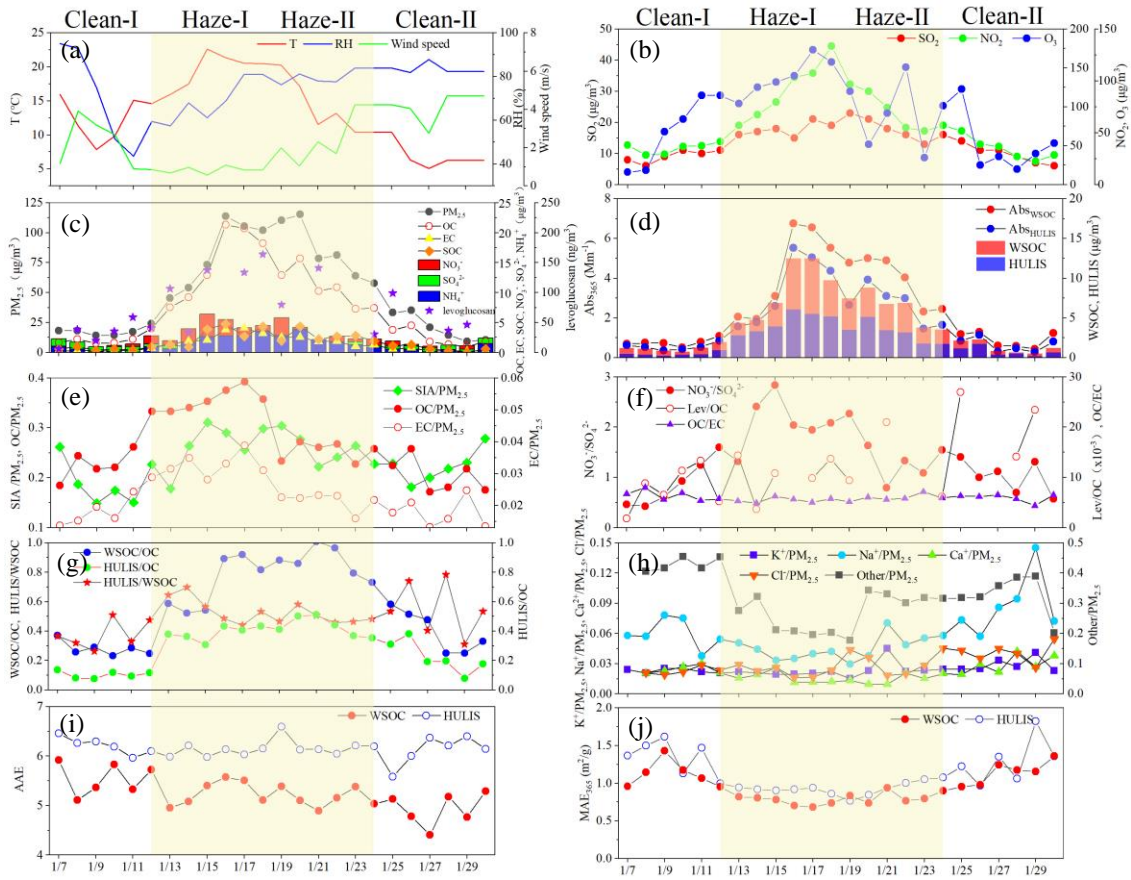
Figure 1. Temporal variation in meteorological parameters, concentrations of chemical composition, and optical properties (Abs$_{365}$, MAE$_{365}$, and AAE) of water-soluble BrC in the PM$_{2.5}$ samples.
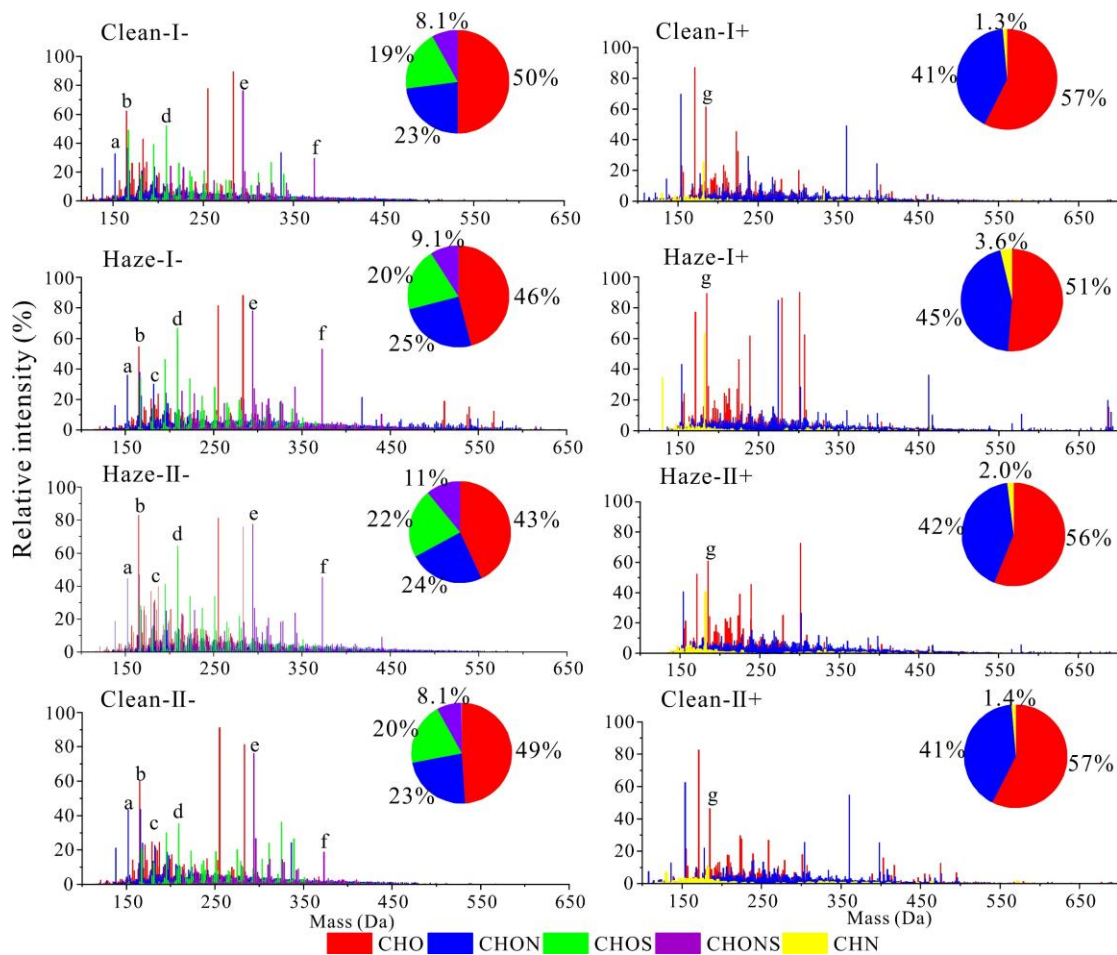
Figure 2. Mass spectra of HULIS detected in ESI- and ESI+ modes during the haze process. The pie charts represent the intensity percent of different compound groups.
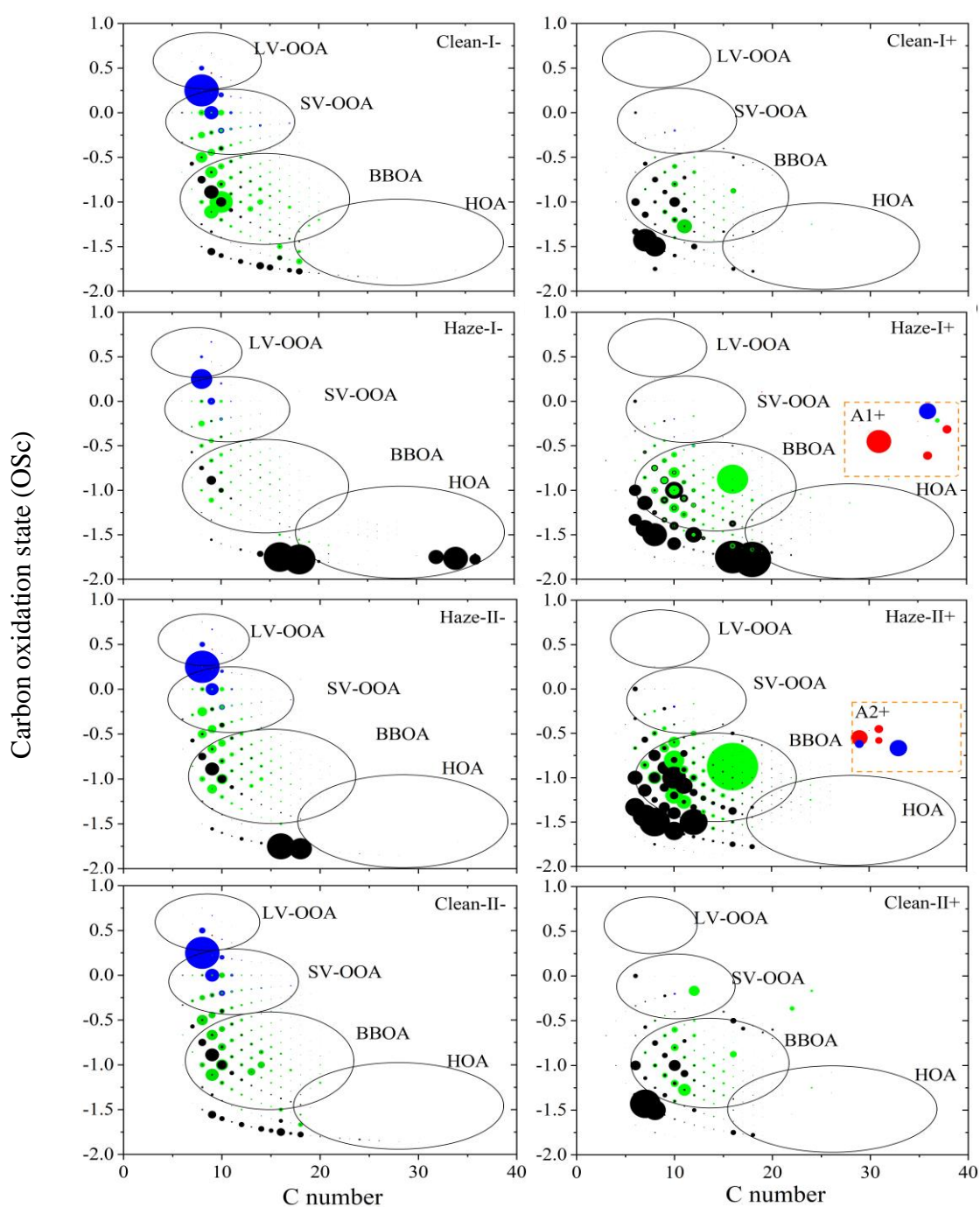
Figure 3. Carbon oxidation state (OSc) plots for CHO- and CHO+. Formulas with black, green, blue, and red are assigned to aliphatic (AI = 0), olefinic (0< AI <0.5), aromatic (0.5≤ AI <0.67), and condensed aromatic (AI ≥0.67) species (Koch and Dittmar, 2006), respectively.
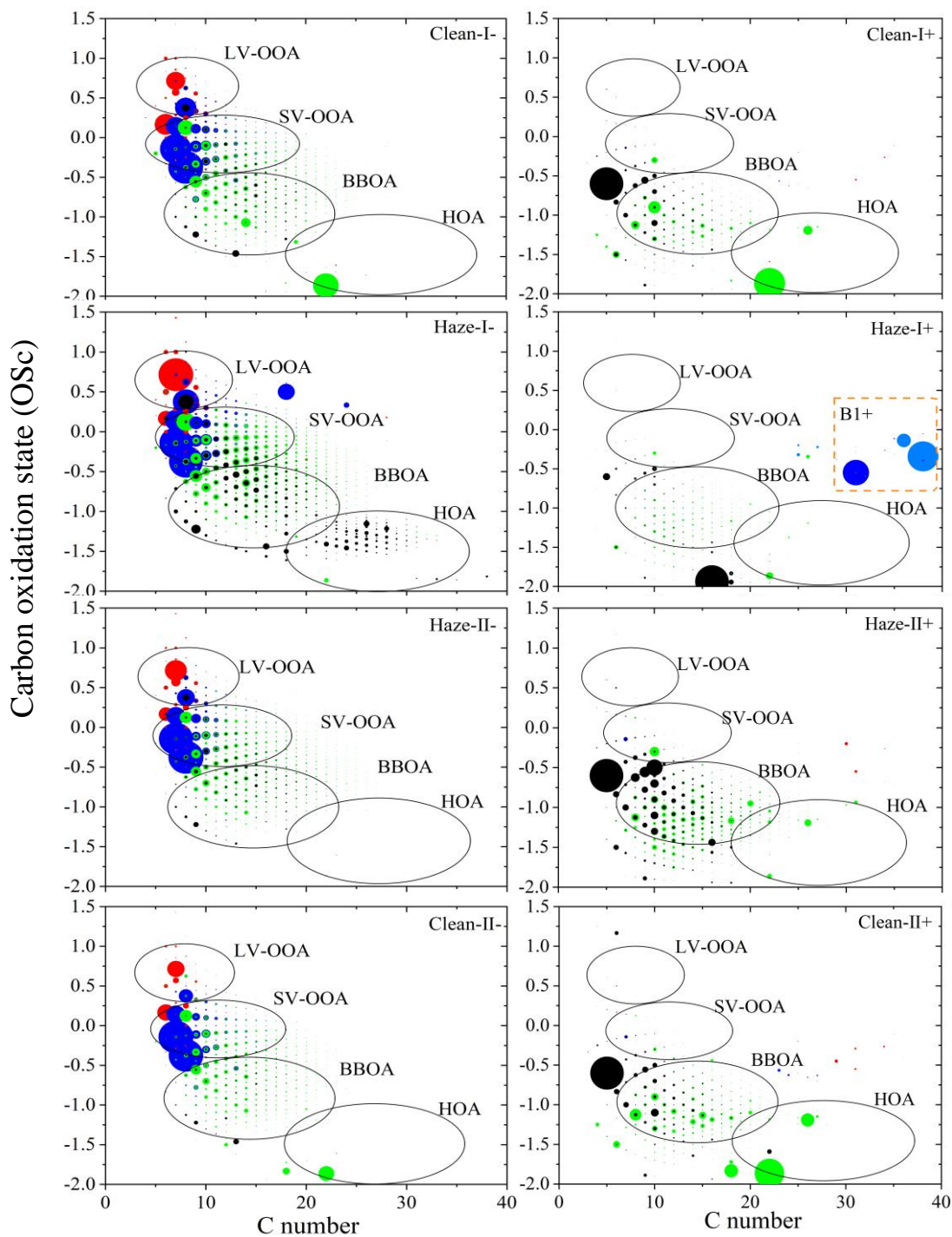
Figure 4. Carbon oxidation state (OSc) plots for CHON- and CHON+. Formulas with black, green, blue, and red are assigned to aliphatic (AI = 0), olefinic (0< AI <0.5), aromatic (0.5≤ AI <0.67), and condensed aromatic (AI ≥0.67) species (Koch and Dittmar, 2006), respective.

1050
1051
1052
1053
1054
1055
1056
1057
1058
1059
1060
1061
1062
1063
1064
1065
1066
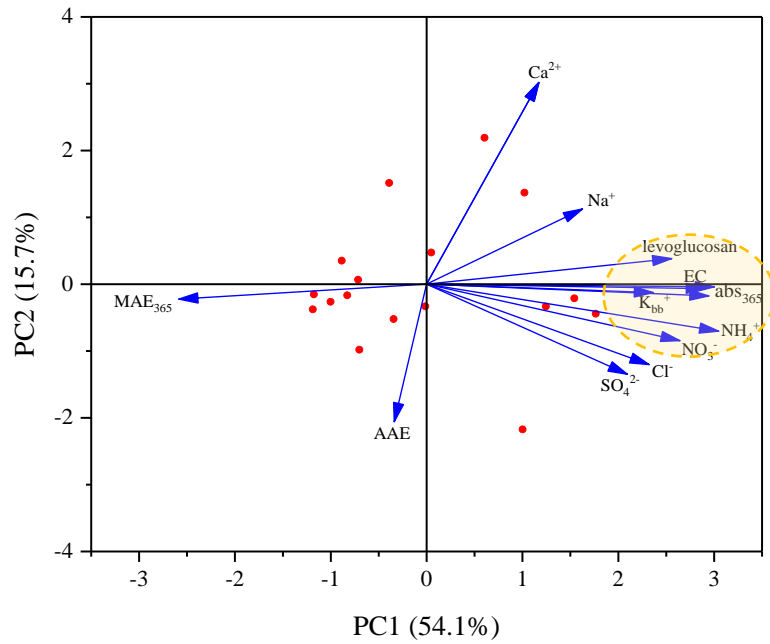
1067 **Figure 5.** Principal component analysis results for the optical properties of HULIS and
1068 chemical compositions of $PM_{2.5}$.
1069